Surface & Coatings Technology 539 (2026) 133892

Contents lists available at ScienceDirect

Surface & Coatings Technology

journal homepage: www.elsevier.com/locate/sct

Full length article

Vacancy-concentration-dependent thermal stability of fcc-(Ti,Al)N_x predicted via chemical-environment-sensitive diffusion activation energies☆

Ganesh Kumar Nayak [a],*, David Holec [b], Jochen M. Schneider [a]

[a] Materials Chemistry, RWTH Aachen University, Kopernikusstr. 10, D-52074 Aachen, Germany
[b] Department of Materials Science, Montanuniversität Leoben, Franz-Josef-Strasse 18, A-8700, Leoben, Austria

ARTICLE INFO

Keywords:
Protective coatings
Titanium aluminium nitride
Diffusion
Nudged elastic band
Density functional theory
Thermal stability

ABSTRACT

The thermal stability of metastable face-centered cubic (fcc) (Ti,Al)N_x coatings is controlled by mass transport, yet the influence of point defects on diffusion barriers remains systematically unexplored. Here, chemical-environment-dependent activation energies are predicted for the first time using density functional theory with systematic configurational sampling in fcc-$(Ti_{0.5}Al_{0.5})_{1-x}N_x$ ($x = 0.43, 0.46, 0.5, 0.53$). We reveal a chemical-environment-dependent activation-energy envelope that single-value estimates cannot capture. Stoichiometric compositions exhibit the highest stability as indicated by the highest activation energies for diffusion, whereas metal and nitrogen vacancies significantly enhance diffusion. These results show that defect-controlled activation-energy variability is essential for designing and synthesizing more thermally robust coatings.

1. Introduction

The service life of face-centered cubic (fcc)-(Ti,Al)N_x industrial protective hard coatings is, among other factors, limited by thermally induced decomposition of the metastable solid solution into fcc and hexagonal close-packed (hcp) phases [1] via spinodal decomposition [2–5]. At around 1000 °C, fcc-Al rich domains, formed during spinodal decomposition, transform into hcp, resulting in a concurrent volume increase that can lead to cracking [1,4]. To enhance the thermal stability of fcc-(Ti,Al)N_x, one research direction has focused on point defect engineering [6–8]. However, the impact of point defects on thermal stability remains a topic of debate, with conflicting findings reported.

Alling et al. [7] reported that the mixing enthalpy of stoichiometric $Ti_{1-y}Al_yN_{1-x}$ is positive but decreases with increasing N vacancy concentration at high Ti content. At high Ti content, introducing N vacancies reduces the mixing enthalpy due to the strong chemical preference of N vacancies to cluster around Ti-rich regions. In contrast, at high Al content, N vacancies increase the mixing enthalpy. Schramm et al. [9] observed that the onset of phase separation is shifted to higher temperatures when reducing the N content in fcc-$Ti_{1-y}Al_yN_x$ coatings with $y = 0.48 - 0.60$ and claimed that this trend is consistent with the reduction in mixing enthalpy predicted by Alling et al. [7]. Conversely, to Baben et al. [6] have shown that actively reducing point defects (both metal and N) is critical to achieve high thermal stability. While the energetics of the decomposition process are comparatively well described [1–7], its kinetic aspects have only been explored in a limited number of studies [6,8].

Grönhagen et al. [8] concluded, based on decomposition kinetics phase-field modeling, that the onset temperature of spinodal decomposition decreases with increasing vacancy concentration. In that study, only metal vacancies were considered, and the diffusion of Al and Ti was modeled during spinodal decomposition only for vacancy concentrations of 10^{-6} and 10^{-5}. They reported that Al diffuses faster than Ti due to the asymmetric curvature of the Gibbs energy curve of vacancies, which is larger on the Al-rich side, even though the diffusivities of Al and Ti were assumed to be equal in the model. The formation of the hcp phase was not considered in this study.

Utilizing a correlative theoretical and experimental research strategy, to Baben et al. [6] related the population of point defects to diffusivity and therefore thermal stability. The authors report that the thermal stability of close-to-stoichiometric (Ti,Al)N thin films was significantly highger compared to over- and understoichiometric variants. Using *ab initio* calculations to determine point defect energies combined with thermodynamic modeling of defect concentrations under varying reactive gas partial pressures, the enhanced thermal stability of the (Ti,Al)N variant with minimized point defects was explained: this variant exhibited a diffusivity reduced by 12 orders of magnitude compared to the variant with the highest defect concentration [6]. The

☆ This article is part of a Special issue entitled: 'Functional Materials' published in Surface & Coatings Technology.

* Corresponding author.
E-mail addresses: nayak@mch.rwth-aachen.de (G.K. Nayak), david.holec@unileoben.ac.at (D. Holec), schneider@mch.rwth-aachen.de (J.M. Schneider).

https://doi.org/10.1016/j.surfcoat.2026.133892
Received 9 April 2026; Received in revised form 14 July 2026; Accepted 2 September 2026
Available online 15 September 2026
0257-8972/© 2026 The Authors. Published by Elsevier B.V. This is an open access article under the CC BY license (http://creativecommons.org/licenses/by/4.0/).
Open access funding enabled and organized by Projekt DEAL.

kinetic aspects of this study were based on calculating the diffusion migration energy for one selected migration pathway only (single-point-calculated), despite the presence of numerous variations in the chemical environment. While a single-point-calculated activation energy is relevant for the corresponding chemical environment, it cannot capture the complex variations in chemical environments in a metastable solid solution crystal in the presence of point defects.

The objective of this work is to unravel the effect of point defects on the thermal stability of fcc-(Ti,Al)N_x, explicitly accounting for the intrinsic variability of chemical-environment-sensitive diffusion activation energies for the first time. We focus on the fcc-$Ti_{0.5}Al_{0.5}N$ composition as it represents one of the technologically important compositions within the TiAlN coating system and has an excellent balance between high hardness, fracture resistance, oxidation resistance, and thermal stability, making it widely used for high-performance cutting tools [10]. Furthermore, the metastable $Ti_{0.5}Al_{0.5}N$ is located well within the cubic solid-solution stability range while remaining close to the composition range where phase separation and the cubic-to-wurtzite transition become increasingly important, providing an excellent opportunity to study the interplay between thermodynamics and kinetics [11]. The activation energies (E_a) are evaluated from the vacancy formation energies (E_f) and the diffusion migration energy barriers (E_b), using a computational approach previously introduced as the "envelope" method: this method, based on 0 K density functional theory (DFT) calculations, was previously employed to predict the Al-rich domain in stoichiometric (V,Al)N [12] and to investigate the underlying interplay among local chemistry, kinetics and lattice distortion in stoichiometric, chemically complex nitrides [13].

2. Methods and computational details

As revealed by to Baben et al. [14], metal vacancies enable N overstoichiometry, while N vacancies lead to N understoichiometry. It has been shown before that the concentration of vacancies in fcc-B1 random alloys is remarkably higher than that of the other defects, such as interstitials and anti-sites [15]. Therefore, both types of (structural) vacancies were included in our calculations. We considered four different cases of fcc-$(Ti_{0.5}Al_{0.5})_{1-x}N_x$ with x = 0.43, 0.46, 0.5 and 0.53, which represent two under-stoichiometric, stoichiometric, and over-stoichiometric compositions, respectively (see schematics in Fig. 1(a)). The structures are based on a 64-site fcc-B1 supercell, comprising separate metal (Ti and Al) and N sublattices, each containing 32 atoms in the defect-free configuration. To obtain the target compositions, the special quasi-random structure (SQS) method [16] was employed to model random solid solutions by distributing metals with and without vacancies, or N with and without vacancies, across their respective sublattices, using the SQSgenerator code [17]. The considered supercell size represents a compromise between computational expense and configurational sampling. Using cluster expansion analysis, Tasnádi et al. [18] showed that vacancy formation energies, E_f, in TiAlN depend primarily on the configuration of the first and second coordination shells surrounding the vacancy. Therefore, the essential local chemical interactions are captured with the present model. To this end, vacancies are introduced into the fcc-$(Ti_{0.5}Al_{0.5})_{1-x}N_x$ with $x = 0.5$ configuration containing 32 metal and 32 N sites to calculate the E_f of a particular vacancy in a particular chemical environment (see Fig. 1(b)) building on the method employed for stoichiometric configurations from [12,13]:

$$E_f = E_i - E_0 + \mu_i \quad (1)$$

where E_i and E_0 are the total energies of the supercell with and without the vacancy, respectively, and μ_i is the chemical potential of the species i. The reference energy for each element was conventionally set to the energy per atom in its most stable form: fcc-A1-Al, hcp-A3-Ti, and the N_2 molecule. Consequently, 64 individual vacancy calculations were performed for each system. Vacancy formation energies were

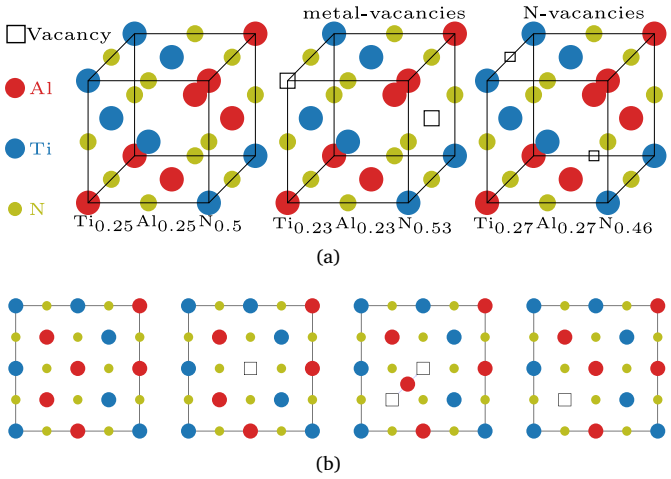


Fig. 1. Schematic representations of (a) (left to right) stoichiometric, overstoichiometric, and understoichiometric structures without, with metal, and with N vacancies, respectively. (b) Example of a migration pathway for Al: (left to right) original bulk structure, single vacancy in the initial configuration, atom in a transition state with two effective nearby vacancies, and final state with a single vacancy (migration completed).

calculated with respect to elemental Ti, Al, and N_2 reference reservoirs. These values provide a consistent basis for comparing defect energetics and are commonly used in the literature [14,19,20]; however, they should not be interpreted directly as equilibrium thermal vacancy formation energies under service conditions, where the effective chemical potentials are governed by local reservoirs such as surfaces, grain boundaries, dislocations, or decomposed Ti-rich/Al-rich domains, which would influence the particular choice of the chemical potentials μ_i [21,22].

Subsequently, diffusion migration energy barriers, E_b, dependent on the local chemical environment, were calculated using the nudged elastic band (NEB) method [23]. These calculations reveal the likelihood of atomic migration between neighboring sites, offering insight into the feasibility of diffusion in chemically varied regions within the solid solution. Thereby, the envelope approach [12,13] ensures that an atom migrates to a vacant site only if that site was originally occupied by the same atomic species in the parent (vacancy-free) supercell. This constraint enhances computational efficiency by allowing all configurations to be systematically derived from a single parent structure.

To compute the vacancy formation energy, E_f, and migration barrier, E_b, we employed the DFT as implemented in the Vienna *Ab initio* Simulation Package (VASP) [24,25]. While the computational methodology for the vacancy-free supercell, in terms of chemical environment, follows our previous work [12,13], the approach for vacancy-containing parent configurations with x = 0.43, 0.46, 0.53 differs by explicitly accounting for preexisting vacancies. The estimation of E_f was achieved as described above; for instance, the $x = 0.53$ configuration contains 32 metal sites, 28 of which are occupied by metals and 4 by vacancies, along with 32 N sites; the $x = 0.46$ configuration contains 28 N sites along with 4 vacancies; and the x = 0.43 configuration contains 24 N sites along with 8 vacancies, among 32 N sites.

Similar to the stoichiometric case, an atom migrates to a vacant site only if that site was originally occupied by the same atomic species in the parent vacancy-containing supercell. This particularly means that we do not consider hops of atoms into a neighboring structural vacancy, for the same reason as we exclude hops between thermal vacancies of different metals. All the parent supercells, i.e., both vacancy-free and vacancy-containing, were relaxed regarding size, shape, and atomic

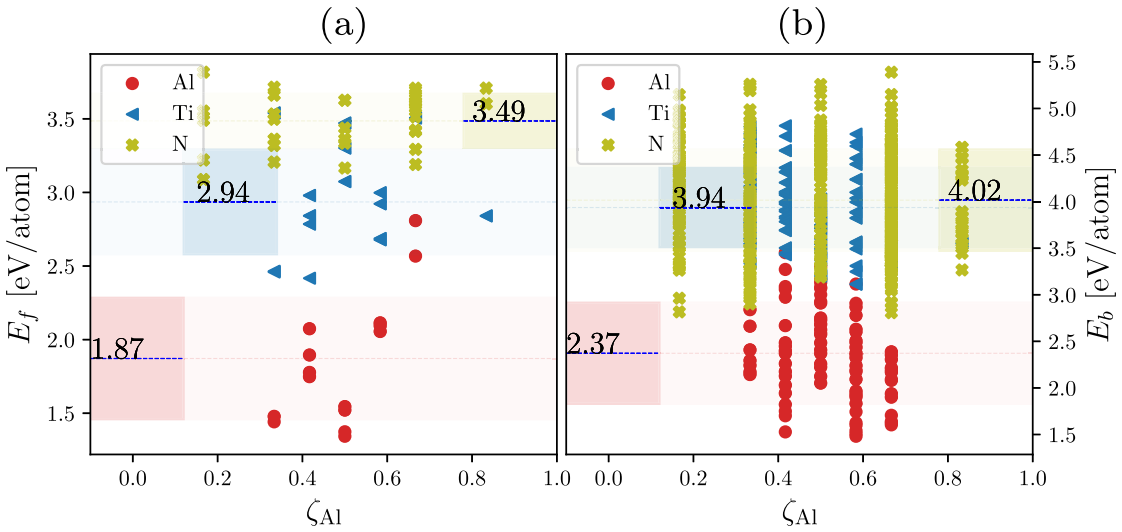


Fig. 2. Envelopes for (a) vacancy formation energies (E_f) and (b) diffusion migration energies (E_b) of all species for fcc-$Ti_{0.25}Al_{0.25}N_{0.5}$, plotted as a function of the fraction of Al neighbors, ζ_{Al}, which occupy the 1st nearest neighbor sites (1NN) of N atoms and the 2nd nearest neighbor sites (2NN) for metal atoms.

positions, whereas for estimation of E_f the supercells were relaxed regarding only atomic positions and with the volume of the parent supercell. Within our model, the off-stoichiometric models contain multiple vacancies within the same supercell. It is shown that the vacancy–vacancy interaction in nirides has a negligible impact on the vacancy formation energies [26] as well as the diffusivity [27]. The computation of E_b follows the same constraint as above, except that additional preexisting vacancies are available. Fig. 1(b) shows the creation of a vacancy in bulk, and the related migration pathways.

The electron–electron exchange and correlation interactions were described by the GGA-PBE [28] parametrization. The recommended pseudopotentials (Ti_sv, Al, N) from the VASP website were used for each element in the calculations, treating any semi-core states as valence states. The projector-augmented-wave method [29] was used to describe the ion–electron interactions, with a plane-wave energy cutoff of 500 eV. The corresponding Brillouin zone was sampled with a 6 × 6 × 6 Monkhorst–Pack k-point mesh [30]. The Methfessel–Paxton [31] smearing of 0.2 eV was applied. A convergence criterion of 10^{-6} (per supercell) was used for the total energy during the electronic self-consistency cycles and ionic relaxations during structural optimizations, and the total energy convergence of 10^{-4} (per supercell) was applied. All our calculations were non-magnetic.

3. Results and discussion

To establish a reference configuration for discussing the vacancy-concentration-dependent thermal stability, we begin with the fcc-$Ti_{0.25}Al_{0.25}N_{0.5}$ composition, in which the metal sublattice comprises 16 Ti and 16 Al atoms. The calculated lattice parameter is 4.17 Å, closely matching the previously reported value of 4.19 Å [1]. Since compounds with fully populated metal and nonmetal sublattices lack structural vacancies, mass transport relies solely on thermally generated vacancies. The energies required to form a single vacancy in fcc-$Ti_{0.25}Al_{0.25}N_{0.5}$ are collected in Fig. 2(a), where each species is represented with distinct markers and color codes. Horizontal dotted lines indicate the mean E_f for each species, and shaded regions reflect the standard deviation due to changes in local chemical environment across the solid solution expressed as the fraction of Al neighbors, ζ_{Al}, which occupy the 1st nearest neighbor sites (1NN) of N atoms and the 2nd nearest neighbor sites (2NN) for the metal atoms. This graphical representation, which captures the impact of chemical variability on vacancy formation energies, is consistently applied to all subsequent compositions discussed. The formation energies of metal species seem, in general, to increase with increasing ζ_{Al}, i.e., enriching the local environment with Al. This is an identical trend as reported in Ref. [18]. Furthermore, our calculated E_fs are comparable to those reported by Tasnádi et al. [18] for $Ti_{0.25}Al_{0.25}N_{0.5}$ containing realistic short-range order (SRO). Although we did not perform the E_f corrections for changed composition and SRO upon vacancy creation, the predicted variation in vacancy formation energies across all atomic sites is similar in the present study to that in Ref. [18] with the min–max spread in the range of 1–2 eV, underscoring their strong sensitivity to the local chemical environment. We also note that Ti vacancy formation energy is slightly smaller than what has been reported for pure TiN (E_f(Ti) = 3.3 eV [32]), which, however, falls into the span calculated here for various chemical environments (2.42 – 3.54 eV). Similarly, the mean barriers for Ti and N in TiAlN, both very close to 4 eV, are well in agreement with those reported for pure TiN [33]. On the contrary to pure TiN, however, the ternary TiAlN system exhibits a significant spread of those values depending on the local chemical environment, making the present case qualitatively different from pure TiN.

As shown in Fig. 2(a), in fcc-$Ti_{0.25}Al_{0.25}N_{0.5}$, Al exhibits the lowest E_f among all species, making Al vacancies the most likely to form during heat treatment. The primary formation of an Al-rich region has been shown experimentally in many studies [6,34]. While the absolute values of E_f remain susceptible to the actual choice of chemical potentials in Eq. (1) and hence to the representative reservoirs, the agreement with experimental observation suggests that the present choice may be plausible. N vacancies require even higher energies and appear only with further thermal activation.

Fig. 2(b) presents the corresponding E_b envelopes, representing the chemical-environment-dependent energy barriers that atoms must overcome to migrate to adjacent vacant lattice sites. From the comparison of the E_b envelope overlaps between the different migrating species, a picture similar to that for the vacancy formation sequence emerges: Al migration is enabled at lower energies than Ti and N. Experimentally, this trend – where Al-rich domains form before Ti-rich regions – has been confirmed via atom probe tomography [6,34]. A straightforward way to analyze and compare the envelopes is to compute mean values from the distributions and assess the width of each distribution via the standard deviation, as well as the difference between the minimum and maximum values in each envelope. These data are compiled in Table 1 for the stoichiometric composition as well as for the metal vacancy containing and the N vacancy containing compositions, while the corresponding envelope data for fcc-$(Ti_{0.5}Al_{0.5})_{1-x}N_x$ with x = 0.43, 0.46, 0.53, formatted as in Fig. 2, can be found in supplementary material as Figures S1, S2, S3, respectively.

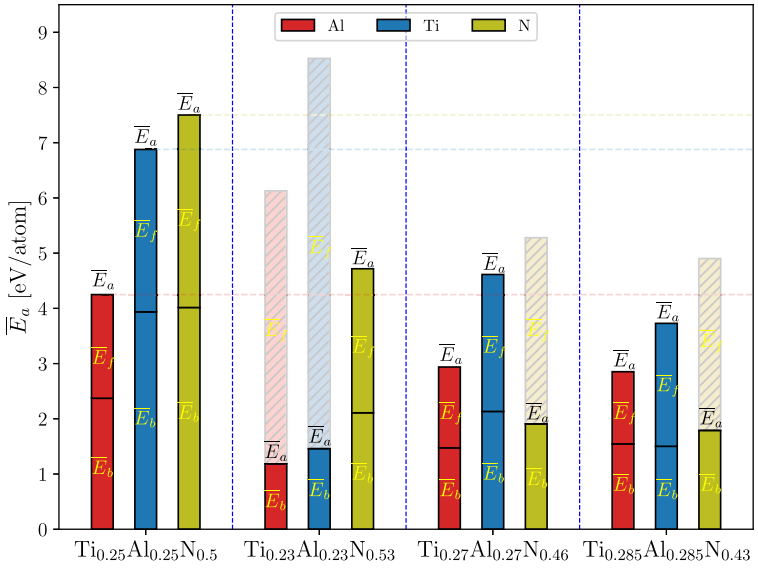


Fig. 3. The mean activation energy for diffusion, $\overline{E}_a$, plotted as the sum of the mean vacancy formation energy, $\overline{E}_f$, and the mean diffusion migration energy, $\overline{E}_b$, for all species and all here considered compositions. Dashed regions indicate compositions for which migration does not require thermal vacancy generation.

Table 1
The minimum values (Min), mean (Mean), maximum (Max) values, and standard deviation (Std) of vacancy formation energies, E_f, diffusion migration energies, E_b.

Composition	Energies [eV/atom]	Metric	Al	Ti	N
$Ti_{0.25}Al_{0.25}N_{0.5}$	E_f	Min	1.34	2.42	3.08
		Mean	1.87	2.94	3.49
		Max	2.81	3.54	3.82
		Std	0.41	0.35	0.18
	E_b	Min	1.48	3.11	2.81
		Mean	2.37	3.94	4.02
		Max	3.45	4.81	5.39
		Std	0.54	0.42	0.54
$Ti_{0.23}Al_{0.23}N_{0.53}$	E_f	Min	3.64	6.08	1.71
		Mean	4.94	7.07	2.61
		Max	5.95	8.07	3.14
		Std	0.64	0.53	0.35
	E_b	Min	−1.31	−1.13	−1.13
		Mean	1.18	1.46	2.11
		Max	3.25	4.73	5.19
		Std	1.10	1.48	1.56
$Ti_{0.27}Al_{0.27}N_{0.46}$	E_f	Min	0.93	1.86	2.59
		Mean	1.46	2.48	3.37
		Max	2.02	3.21	3.97
		Std	0.32	0.32	0.26
	E_b	Min	−0.70	−0.62	−0.68
		Mean	1.47	2.13	1.91
		Max	2.94	4.82	5.79
		Std	1.00	1.58	1.68
$Ti_{0.285}Al_{0.285}N_{0.43}$	E_f	Min	0.94	1.62	2.45
		Mean	1.31	2.23	3.11
		Max	1.71	2.60	3.72
		Std	0.22	0.33	0.32
	E_b	Min	−0.28	−0.86	−0.73
		Mean	1.55	1.50	1.79
		Max	3.24	4.66	5.18
		Std	0.78	1.58	1.39

In Fig. 3, the predicted mean activation energy for diffusion ($\overline{E}_a$) [13] is presented for each species and composition considered, where $\overline{E}_a = \overline{E}_f + \overline{E}_b$, with $\overline{E}_f$ denoting the mean vacancy formation energy and $\overline{E}_b$ the corresponding mean migration barrier. Dashed regions mark compositions where structural vacancies are readily available in the system and hence no thermally generated vacancies are necessary for the migration. In Fig. 3, the effect of introducing metal vacancies on the migration energetics is revealed. When metal vacancies are introduced into the crystal structure of the stoichiometric compound, the mean activation energy for diffusion, $\overline{E}_a$, is reduced to the mean migration barrier, $\overline{E}_b$, for both Al and Ti. This substantial reduction – by approximately 72% for Al and 78% for Ti – occurs because thermal vacancy generation is no longer required for atomic migration, as pre-existing metal vacancies that accommodate the N overstoichiometry enable migration. In addition, the magnitude of $\overline{E}_b$ is reduced relative to that in the stoichiometric configuration. This significant decrease – by 50% for Al and 62% for Ti – is likely attributable to the relaxation of local lattice strain surrounding the metal vacancies, thereby accelerating metal migration and hence, decomposition.

Similarly, the introduction of N vacancies leads to a decrease in the mean migration barrier for both Al and Ti relative to the stoichiometric variant. This decrease is also likely a result of local lattice strain relaxation near the N vacancies, which facilitates atomic movement by reducing migration resistance and thereby decreasing thermal stability compared to fcc-$Ti_{0.25}Al_{0.25}N_{0.5}$. An increase in the concentration of metal or N vacancies leads, hence, to a noticeable decrease in thermal stability, as demonstrated by the changes in the maximum diffusion activation energies of Al and Ti within fcc-$Ti_{0.25}Al_{0.25}N_{0.5}$. The predicted reduction in thermal stability – and the associated decrease in decomposition temperature – indicates that metal and N vacancies critically facilitate atomic mobility in the here investigated nitrides.

We note that the evaluation of the vacancy formation energy, E_f, as presented in this study, is simplified by omitting operative reservoirs such as grain boundaries or decomposed Ti-rich/Al-rich domains and by neglecting finite-size effects [18]. Physically meaningful E_f values for vacancies, as structural defects, are positive values. Importantly, even in the limiting case of $\overline{E}_f \rightarrow 0$, i.e., $\overline{E}_a = \overline{E}_b$, the largest barriers and hence the expected lowest mobility of all species are in the stoichiometric case (cf. Fig. 3).

At temperatures relevant to spinodal decomposition, the vacancy formation free energies and stability of $Ti_{1-x}Al_xN$ also include configurational (stabilizes the solid solution) and vibrational entropy contributions which can substantially modify the Ti–Al–N miscibility gap [35,

36]. We note that both E_f and E_b were calculated at 0 K and therefore explicit finite-temperature effects may play a role at high temperatures (relevant to the applications of TiAlN). For example, Sangiovanni [33] showed that the migration barriers of Ti (N) slightly decrease (increase) with T. Such calculations are beyond the scope of the present work. However, let us conclude that the trends are likely to remain qualitatively unchanged, as supported by previous experimental work [6, 34].

Furthermore, high-diffusivity paths, such as grain or column boundaries, may be followed within the grains and contribute to the overall kinetics of practical $Ti_{1-x}Al_xN$ coatings [8,37]. In columnar PVD coatings, grain boundaries can provide faster diffusion paths due to their lower atomic packing density (and hence related lower migration barriers [38]) and higher defect concentration. However, bulk diffusion is a prominent mechanism in the kinetic pathway. The present results should be regarded as describing the intrinsic lattice diffusion behavior, while the overall thermal stability of real coatings will also depend on microstructural features such as grain size, grain-boundary character, and coating density.

Consequently, stoichiometric fcc-$Ti_{0.25}Al_{0.25}N_{0.5}$ is predicted to exhibit the highest thermal stability, a conclusion that aligns well with existing experimental data reported in the literature [6]. Fully populated metal and nonmetal sublattices thus appear essential for optimizing the thermal stability of these materials. Analysis of the widths of the predicted energy envelopes reveals a strong dependence of both vacancy formation energies, E_f, and migration barriers, E_b, on the local chemical environment. This variability – exemplified by the differences between the minimum and maximum values within one envelope (see Fig. 2, Table 1, and Figures S1, S2, and S3) – underscores the complexity of atomic migration processes in these materials. It also suggests that activation energy values reported in the literature based on isolated or "single point" calculations may fail to capture the influence of chemical-environment heterogeneity on diffusion behavior and, consequently, thermal stability.

4. Conclusion

In summary, the thermal stability relevant formation energies for vacancies and the corresponding barriers for migration for stoichiometric fcc-$Ti_{0.25}Al_{0.25}N_{0.5}$ have been predicted and compared to variants containing metal vacancies and N vacancies while accounting for the inherent variability of chemical environment. The results can be summarized as follows:

- An increase in metal or N vacancy concentration lowers the decomposition temperature, as indicated by the mean diffusion activation energy of Al and Ti in fcc-$Ti_{0.25}Al_{0.25}N_{0.5}$.
- Thus, the stoichiometric compound is predicted to exhibit maximum thermal stability, consistent with experimental literature data [6].
- The introduction of metal vacancies in the structures reduces the magnitude of the mean activation energy for diffusion, $\overline{E}_a$, to the mean migration barrier, $\overline{E}_b$, for both Al and Ti, as thermal vacancy generation is not required for migration. Furthermore, the magnitude of $\overline{E}_b$ is reduced compared to the stoichiometric configuration, likely due to relaxation of local lattice strain in the vicinity of the point defects, thereby accelerating migration.
- From the analysis of the width of each envelope predicted here, it is evident that the magnitude of both E_f and E_b is very strongly chemical-environment-dependent. Therefore, literature reports based on "single point" activation energy data cannot reflect the complex impact of the chemical environment on the migration behavior.

CRediT authorship contribution statement

Ganesh Kumar Nayak: Writing – review & editing, Writing – original draft, Visualization, Validation, Methodology, Investigation, Formal analysis, Conceptualization. **David Holec:** Writing – review & editing, Supervision, Conceptualization. **Jochen M. Schneider:** Writing – review & editing, Validation, Supervision, Conceptualization.

Funding

GKN and JMS gratefully acknowledge the Ministry for Culture and Science of the State of North Rhine-Westphalia (MKW NRW) for supporting this work as part of the NHR funding. The authors also gratefully acknowledge the computing time provided to them on the high-performance computer CLAIX at the NHR Center NHR4CES with project ID p0020883.

Declaration of competing interest

The authors declare the following financial interests/personal relationships which may be considered as potential competing interests: Ganesh Kumar Nayak reports financial support was provided by RWTH Aachen University. If there are other authors, they declare that they have no known competing financial interests or personal relationships that could have appeared to influence the work reported in this paper.

Acknowledgments

The authors highly acknowledge open-access software packages VESTA [39] and pymatgen [40] for supporting the visualization and processing of the structures.

Appendix A. Supplementary data

Supplementary material related to this article can be found online at https://doi.org/10.1016/j.surfcoat.2026.133892.

Data availability

Data will be made available on request.

References

[1] P.H. Mayrhofer, A. Hörling, L. Karlsson, J. Sjölén, T. Larsson, C. Mitterer, L. Hultman, Self-organized nanostructures in the Ti–Al–N system, Appl. Phys. Lett. 83 (10) (2003) 2049–2051, http://dx.doi.org/10.1063/1.1608464.
[2] P.H. Mayrhofer, D. Music, J.M. Schneider, Ab initio calculated binodal and spinodal of cubic $Ti_{1-x}Al_xN$, Appl. Phys. Lett. 88 (7) (2006) 071922, http://dx.doi.org/10.1063/1.2177630.
[3] N. Norrby, M.P. Johansson, R. M'Saoubi, M. Odén, Pressure and temperature effects on the decomposition of arc evaporated $Ti_{0.6}Al_{0.4}N$ coatings in continuous turning, Surf. Coat. Technol. 209 (2012) 203–207, http://dx.doi.org/10.1016/j.surfcoat.2012.08.068.
[4] P.H. Mayrhofer, R. Rachbauer, D. Holec, F. Rovere, J. Schneider, Protective transition metal nitride coatings, Comprehensive Materials Proceedings, vol. 4, 2014, pp. 355–388, http://dx.doi.org/10.1016/B978-0-08-096532-1.00423-4.
[5] D. Music, R.W. Geyer, J.M. Schneider, Recent progress and new directions in density functional theory based design of hard coatings, Surf. Coat. Technol. 286 (2016) 178–190, http://dx.doi.org/10.1016/j.surfcoat.2015.12.021.
[6] M. to Baben, M. Hans, D. Primetzhofer, S. Evertz, H. Ruess, J.M. Schneider, Unprecedented thermal stability of inherently metastable titanium aluminum nitride by point defect engineering, Mater. Res. Lett. 5 (3) (2017) 158–169, http://dx.doi.org/10.1080/21663831.2016.1233914.
[7] B. Alling, A. Karimi, L. Hultman, I.A. Abrikosov, First-principles study of the effect of nitrogen vacancies on the decomposition pattern in cubic $Ti_{1-x}Al_xN_{1-y}$, Appl. Phys. Lett. 92 (7) (2008) 071903, http://dx.doi.org/10.1063/1.2838747.
[8] K. Grönhagen, J. Ågren, M. Odén, Phase-field modelling of spinodal decomposition in TiAlN including the effect of metal vacancies, Scr. Mater. 95 (2015) 42–45, http://dx.doi.org/10.1016/j.scriptamat.2014.09.027.

[9] I. Schramm, M.J. Jõesaar, J. Jensen, F. Mücklich, M. Odén, Impact of nitrogen vacancies on the high temperature behavior of $(Ti_{1-x}Al_x)N_y$ alloys, Acta Mater. 119 (2016) 218–228, http://dx.doi.org/10.1016/j.actamat.2016.08.024.

[10] A. Hörling, L. Hultman, M. Odén, J. Sjölén, L. Karlsson, Mechanical properties and machining performance of $Ti_{1-x}Al_xN$-coated cutting tools, Surf. Coat. Technol. 191 (2–3) (2005) 384–392, http://dx.doi.org/10.1016/j.surfcoat.2004.04.056.

[11] Y. Zhang, P. Franke, H.J. Seifert, CALPHAD modeling of metastable phases and ternary compounds in Ti-Al-N system, Calphad 59 (2017) 142–153, http://dx.doi.org/10.1016/j.calphad.2017.09.006.

[12] M. Hans, Z. Czigány, D. Neuß, J.A. Sälker, H. Rueß, J. Krause, G.N. Nayak, D. Holec, J.M. Schneider, Probing the onset of wurtzite phase formation in (V,Al)N thin films by transmission electron microscopy and atom probe tomography, Surf. Coat. Technol. 442 (2022) 128235, http://dx.doi.org/10.1016/j.surfcoat.2022.128235.

[13] G.K. Nayak, A. Kretschmer, P.H. Mayrhofer, D. Holec, On correlations between local chemistry, distortions and kinetics in high entropy nitrides: An ab initio study, Acta Mater. 255 (2023) 118951, http://dx.doi.org/10.1016/j.actamat.2023.118951.

[14] M. to Baben, L. Raumann, D. Music, J.M. Schneider, Origin of the nitrogen over- and understoichiometry in $Ti_{0.5}Al_{0.5}N$ thin films, J. Phys. Condens. Matter 24 (15) (2012) 155401, http://dx.doi.org/10.1088/0953-8984/24/15/155401.

[15] M. Mühlbacher, A.S. Bochkarev, F. Mendez-Martin, B. Sartory, L. Chitu, M.N. Popov, P. Puschnig, J. Spitaler, H. Ding, N. Schalk, J. Lu, H. Lars, C. Mitterer, Cu diffusion in single-crystal and polycrystalline TiN barrier layers: A high-resolution experimental study supported by first-principles calculations, J. Appl. Phy. 118 (8) (2015) 085307, http://dx.doi.org/10.1063/1.4929446.

[16] S. Wei, L.G. Ferreira, J.E. Bernard, A. Zunger, Electronic properties of random alloys: Special quasirandom structures, Phys. Rev. B 42 (15) (1990) 9622–9649, http://dx.doi.org/10.1103/physrevb.42.9622.

[17] D. Gehringer, M. Friák, D. Holec, Models of configurationally-complex alloys made simple, Comput. Phys. Commun. 286 (2023) 108664, http://dx.doi.org/10.1016/j.cpc.2023.108664.

[18] F. Tasnádi, A.V. Lugovskoy, M. Odén, I.A. Abrikosov, Non-equilibrium vacancy formation energies in metastable alloys—A case study of $Ti_{0.5}Al_{0.5}N$, Mater. Des. 114 (2017) 484–493, http://dx.doi.org/10.1016/j.matdes.2016.10.071.

[19] T. Marten, E.I. Isaev, B. Alling, L. Hultman, I.A. Abrikosov, Single-monolayer SiNx embedded in TiN: A first-principles study, Phys. Rev. B 81 (21) (2010) 212102, http://dx.doi.org/10.1103/PhysRevB.81.212102.

[20] H. Euchner, P.H. Mayrhofer, Vacancy-dependent stability of cubic and wurtzite $Ti_{1-x}Al_xN$, Surf. Coat. Technol. 275 (2015) 214–218, http://dx.doi.org/10.1016/j.surfcoat.2015.05.017.

[21] T. Marten, B. Alling, E. Isaev, H. Lind, F. Tasnádi, L. Hultman, I.A. Abrikosov, First-principles study of the SiN_x/TiN(001) interface, Phys. Rev. B 85 (10) (2012) http://dx.doi.org/10.1103/PhysRevB.85.104106.

[22] N. Koutná, D. Holec, O. Svoboda, F.F. Klimashin, P.H. Mayrhofer, Point defects stabilise cubic Mo-N and Ta-N, J. Phys. D Appl. Phys. 49 (37) (2016) 375303, http://dx.doi.org/10.1088/0022-3727/49/37/375303.

[23] D. Sheppard, R. Terrell, G. Henkelman, Optimization methods for finding minimum energy paths, J. Chem. Phys. 128 (13) (2008) 134106, http://dx.doi.org/10.1063/1.2841941.

[24] G. Kresse, J. Furthmüller, Efficiency of ab-initio total energy calculations for metals and semiconductors using a plane-wave basis set, Comput. Mater. Sci. 6 (1) (1996) 15–50, http://dx.doi.org/10.1016/0927-0256(96)00008-0.

[25] G. Kresse, J. Furthmüller, Efficient iterative schemes for ab initio total-energy calculations using a plane-wave basis set, Phys. Rev. B 54 (16) (1996) 11169, http://dx.doi.org/10.1103/PhysRevB.54.11169.

[26] V. Razumovskiy, M. Popov, H. Ding, J. Odqvist, Formation and interaction of point defects in group IVb transition metal carbides and nitrides, Comput. Mater. Sci. 104 (2015) 147–154, http://dx.doi.org/10.1016/j.commatsci.2015.03.042.

[27] C. Teichmann, W. Lengauer, P. Ettmayer, J. Bauer, M. Bohn, Reaction diffusion and phase equilibria in the VN system, Met. Mater. Trans. A 28 (13) (1997) 837–842, http://dx.doi.org/10.1007/s11661-997-1011-8.

[28] J.P. Perdew, K. Burke, M. Ernzerhof, Restoring the density-gradient expansion for exchange in solids and surfaces, Phys. Rev. Lett. 77 (18) (1996) 3865, http://dx.doi.org/10.1103/PhysRevLett.77.3865.

[29] P.E. Blöchl, Projector augmented-wave method, Phys. Rev. B 50 (24) (1994) 17953, http://dx.doi.org/10.1103/PhysRevB.50.17953.

[30] H.J. Monkhorst, J.D. Pack, Special points for Brillouin-zone integrations, Phys. Rev. B 13 (12) (1976) 5188, http://dx.doi.org/10.1103/PhysRevB.13.5188.

[31] M. Methfessel, A.T. Paxton, High-precision sampling for Brillouin-zone integration in metals, Phys. Rev. B 40 (6) (1989) 3616, http://dx.doi.org/10.1103/PhysRevB.40.3616.

[32] G.K. Nayak, M.N. Popov, D. Holec, Pressure- and temperature-dependent diffusion from first-principles: A case study of V and Ti in a TiN matrix, Surf. Coat. Technol. 422 (2021) 127491, http://dx.doi.org/10.1016/j.surfcoat.2021.127491.

[33] D.G. Sangiovanni, Mass transport properties of quasiharmonic vs. Anharmonic transition-metal nitrides, Thin Solid Films 688 (2019) 137297, http://dx.doi.org/10.1016/j.tsf.2019.05.016.

[34] D.M. Holzapfel, D. Music, M. Hans, S. Wolff-Goodrich, D. Holec, D. Bogdanovski, M. Arndt, A.O. Eriksson, K. Yalamanchili, D. Primetzhofer, et al., Enhanced thermal stability of (Ti,Al)N coatings by oxygen incorporation, Acta Mater. 218 (2021) 117204, http://dx.doi.org/10.1016/j.actamat.2021.117204.

[35] N. Shulumba, O. Hellman, Z. Raza, B. Alling, J. Barrirero, F. Mücklich, I.A. Abrikosov, M. Odén, Lattice vibrations change the solid solubility of an alloy at high temperatures, Phys. Rev. Lett. 117 (20) (2016) 205502, http://dx.doi.org/10.1103/PhysRevLett.117.205502.

[36] A. Wang, S.-L. Shang, Y. Du, L. Chen, J. Wang, Z.-K. Liu, Effects of pressure and vibration on the thermal decomposition of cubic $Ti_{1-x}Al_xN$, $Ti_{1-x}Zr_xN$, and $Zr_{1-x}Al_xN$ coatings: A first-principles study, J. Mater. Sci. 47 (21) (2012) 7621–7627, http://dx.doi.org/10.1007/s10853-011-6223-z.

[37] R. Rachbauer, S. Massl, E. Stergar, D. Holec, D. Kiener, J. Keckes, J. Patscheider, M. Stiefel, H. Leitner, P.H. Mayrhofer, Decomposition pathways in age hardening of Ti-Al-N films, J. Appl. Phys. 110 (2) (2011) http://dx.doi.org/10.1063/1.3610451.

[38] M.N. Popov, A.S. Bochkarev, V.I. Razumovskiy, P. Puschnig, J. Spitaler, Point defects at the Σ5(012)[100] grain boundary in TiN and the early stages of Cu diffusion: An ab initio study, Acta Mater. 144 (2018) 496–504, http://dx.doi.org/10.1016/j.actamat.2017.11.005.

[39] K. Momma, F. Izumi, VESTA3 for three-dimensional visualization of crystal, volumetric and morphology data, J. Appl. Crystallogr. 44 (6) (2011) 1272–1276, http://dx.doi.org/10.1107/S0021889811038970.

[40] S.P. Ong, W.D. Richards, A. Jain, G. Hautier, M. Kocher, S. Cholia, D. Gunter, V.L. Chevrier, K.A. Persson, G. Ceder, Python materials genomics (pymatgen): A robust, open-source python library for materials analysis, Comput. Mater. Sci. 68 (2013) 314–319, http://dx.doi.org/10.1016/j.commatsci.2012.10.028.